

1986

Nonadiabatic Theory of Fine-Structure Branching Cross Sections for Na-He, Na-Ne, and Na-Ar Optical Collisions

Linda L. Vahala
Old Dominion University, lvahala@odu.edu

P. S. Julienne

Mark D. Havey
Old Dominion University, mhavey@odu.edu

Follow this and additional works at: https://digitalcommons.odu.edu/ece_fac_pubs

 Part of the [Atomic, Molecular and Optical Physics Commons](#), and the [Physical Chemistry Commons](#)

Repository Citation

Vahala, Linda L.; Julienne, P. S.; and Havey, Mark D., "Nonadiabatic Theory of Fine-Structure Branching Cross Sections for Na-He, Na-Ne, and Na-Ar Optical Collisions" (1986). *Electrical & Computer Engineering Faculty Publications*. 49.
https://digitalcommons.odu.edu/ece_fac_pubs/49

Original Publication Citation

Vahala, L.L., Julienne, P.S., & Havey, M.D. (1986). Nonadiabatic theory of fine-structure branching cross sections for Na-He, Na-Ne, and Na-Ar optical collisions. *Physical Review A (General Physics)*, 34(3), 1856-1868. doi: 10.1103/PhysRevA.34.1856

Nonadiabatic theory of fine-structure branching cross sections for Na-He, Na-Ne, and Na-Ar optical collisions

L. L. Vahala*

Department of Physics, Old Dominion University, Norfolk, Virginia 23508

P. S. Julienne

Molecular Spectroscopy Division, National Bureau of Standards, Gaithersburg, Maryland 20899

M. D. Havey

Department of Physics, Old Dominion University, Norfolk, Virginia 23508

(Received 17 December 1985)

The nonadiabatic close-coupled theory of atomic collisions in a radiation field is generalized to include electron spin and is used to consider the weak-field Na-rare-gas (RG) optical collision $\text{Na}(^2S_{1/2}) + \text{RG} + nh\nu \rightarrow \text{Na}(^2P_j) + \text{RG} + (n-1)h\nu$. The effects of detuning and incident energy on the branching into the atomic Na $3p\ ^2P_{3/2}$ and $3p\ ^2P_{1/2}$ states are examined. The cross sections $\sigma(j)$ are found to have a strong asymmetry between red and blue detuning as well as a complex threshold and resonance structure dependence on energy. A partial cross-section analysis of $\sigma(j)$ shows a significant difference between contributions from states of e and f molecular parity. The theoretically calculated detuning dependence of the branching ratio into each fine-structure state is in good agreement with available experimental data for Na-Ar, Na-Ne, and Na-He, as well as the total absorption coefficient for the production of Na $3p$ atoms. The fine-structure branching ratio for thermal energy collisions shows considerable variation with a rare-gas collision partner, due to the different interaction potentials. For sufficiently high collision energy, the branching approaches a recoil limit which is independent of collision partner.

I. INTRODUCTION

For some time, there has been considerable interest in studying nonadiabatic effects in atomic and molecular collisions. These effects play an essential role in determining final-state distributions in the usual elastic or inelastic scattering between atoms or molecules. More recently, emphasis has been placed on the role of nonadiabatic coupling in determining final-state distributions in photoionization, molecular dissociation, and collisional redistribution of light.¹⁻²⁴ These processes have been broadly termed photofragmentation. The final-state distributions of the photofragments may be conveniently described in terms of the multipoles²⁵ produced among various final states accessible to the system.

In this paper, we consider spin-orbit effects in far-wing collisional redistribution of light for Na-rare-gas systems. In particular, we compute the total cross section $\sigma(j)$ for production of each fine-structure state of the Na $3p$ multiplet by optical collisions with He, Ne, and Ar. We find that the cross section $\sigma(j)$ depends strongly on the interatomic potentials, the degree of detuning from resonance, and the scattering energy. Similar calculations have also been carried out by Kulander and Reberstrost for the Na + Ar system.^{10,11} Our work differs from theirs in that we also calculate the effect of He and Ne perturbers and use a different set of potentials for Na-Ar. We also illustrate how the factorization of the radiative S matrix by a generalized multichannel quantum-defect

analysis¹⁴ leads to considerable insight into the nature of the absorption profile and fine-structure branching.

Before presenting the nonadiabatic close-coupling theory with spin, we give a broad outline of the physical processes by considering nonadiabaticity from the viewpoint of coupling between states using various Hund's-case basis sets.²⁶ We follow this by discussing nonadiabatic collision dynamics in terms of a distorted-wave analysis of the radiative scattering matrix.¹⁴

A. Nonadiabatic collision dynamics: Molecular basis sets and nonadiabatic mixing

Consider the absorption of light during a strong collision, followed by fragmentation of the molecule into electronically excited products:



where A and RG represent the alkali-metal (Na here) and rare-gas atoms, respectively; n is the number of photons of energy $h\nu$ in the incident laser field. The phonon energy $h\nu$ is chosen so that the only energetically allowed outcome of the collision (1) is to leave RG in its ground state while exciting the Na atom (A^*) to its $3p\ ^2P_{1/2}$ and $3p\ ^2P_{3/2}$ states. The Born-Oppenheimer (BO) potentials for the Na-RG systems are shown schematically in Fig. 1. A single-mode laser field of frequency ν causes electronic transitions from free ($E > 0$) states of the molecular $X\Sigma$ ground state to free ($E' > 0$) states of the excited molecu-

lar electronic $A\Pi$ and $B\Sigma$ states. From energy considerations, $E + h\nu = E' + h\nu_0$ with Δ , the detuning from resonant excitation, given by $\Delta = h(\nu - \nu_0)$. With the usual assumptions, the classical Franck-Condon principle tells us that for any particular ν , the electronic transitions occur in the vicinity of the internuclear separation R^* where the difference between the upper and lower potentials equals the excitation frequency ν .²⁷

The BO potentials are just the internuclear-separation (R)-dependent eigenvalues of the electronic part (H^e) of the total molecular Hamiltonian H^{mol} . H^e does not include the spin-orbit (H^{so}) or rotational (H^{rot}) interactions.²⁸ It is convenient to introduce a Hund's case-(a) molecular basis $|JMp;S\Lambda\Sigma\rangle$ to represent the electronic-rotational states. Here J and M are the total and space-

fixed projection of the molecular angular momentum, p the molecular parity, and $\Lambda(\Sigma)$ the magnitude of the projection of the electronic orbital (spin) angular momentum onto the moving, molecule-fixed internuclear axis.²⁸ S is the spin. In the absence of the radiative coupling J , M , and p are strictly conserved during a collision. However, the spin-orbit and rotational interaction parts of the molecular Hamiltonian mix states of different Λ and Σ .²⁹ Thus, in the Hund's case-(a) representation, it is these interactions which give rise to nonadiabatic coupling.

Since the case-(a) Hamiltonian is nondiagonal in spin-orbit coupling and, in particular, is asymptotically nondiagonal, it is often convenient to choose as a basis the Hund's case-(c) representation $|JMp;J_a\Omega\rangle$,^{28,29} where J_a is the atomic electronic angular momentum (which is well defined as $R \rightarrow \infty$) and Ω is the projection of J_a on the internuclear axis. In this basis, the spin-orbit operator H^{so} is diagonal so that the diagonal elements of H^{mol} approach the correct fine-structure splitting as $R \rightarrow \infty$. In case (c), off-diagonal terms proportional to the BO difference potentials mix states of the same Ω , and rotational coupling terms mix states of different Ω . Thus, the case-(c) Hamiltonian is strongly nondiagonal in the small- R regions where far-wing absorption occurs, since the electronic splitting is much larger than the spin-orbit coupling terms. The case-(c) Hamiltonian is also nondiagonal at large R where rotational coupling terms varying as R^{-2} mix states of different Ω and of the same J_a . As $R \rightarrow \infty$, the molecular Hamiltonian is diagonal in the case-(e) representation, $|JMp;J_a l\rangle$,²⁸ where l is the quantum number of relative rotational angular momentum for the two atoms, i.e., $J = J_a + l$. The case-(e) states are the channel states of scattering theory,³⁰ and the scattering boundary conditions are applied to the total wave function expanded in the case-(e) basis. The off-diagonal matrix elements in case (e) are proportional to the BO difference potentials and cause strong coupling, at small internuclear separations, of case-(e) states.³¹

At times, it is convenient to define a basis that is not a pure Hund's case of angular momentum coupling.³² One useful choice is to diagonalize $H^e + H^{\text{so}}$ as a function of R , neglecting the rotational coupling terms. The resulting states have the property that they go to case (c) asymptotically as $R \rightarrow \infty$ and to case (a) at small R where the separation of BO potentials is large compared to the non-diagonal coupling terms. The potentials defined this way provide an adiabatic correlation between the short-range case-(a) states and the long-range case-(c) states. Figure 2 shows these potentials for the Na-Ar system.

Thus, the concept of nonadiabaticity should be discussed in conjunction with the representation of the molecular state. Since the different Hund's bases are connected by unitary transformations, they are formally equivalent for constructing the close-coupled equations. Nevertheless, some representations are more convenient than others in considering the process Eq. (1). For example, for detunings in the far wings of the line profile, the Condon point(s) of stationary phase occur(s) in a region of internuclear separation where the excited-state Hamiltonian matrix is nearly diagonal in the Hund's case-(a) basis. Thus, for far-blue-wing detuning, excitation is to a nearly

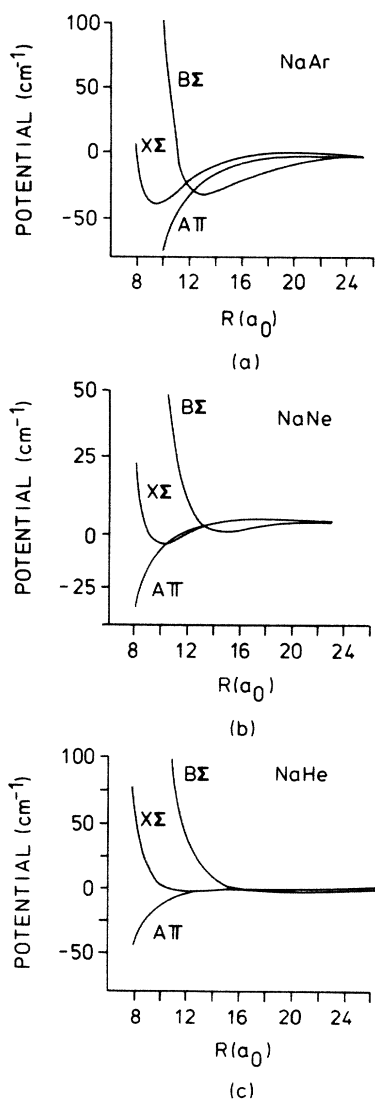


FIG. 1. $X\Sigma$, $A\Pi$, and $B\Sigma$ Born-Oppenheimer potentials for (a) Na-Ar, (b) Na-Ne, and (c) Na-He. The $X\Sigma$ asymptotic energy has been shifted to coincide with that of the $A\Pi$ and $B\Sigma$ states.

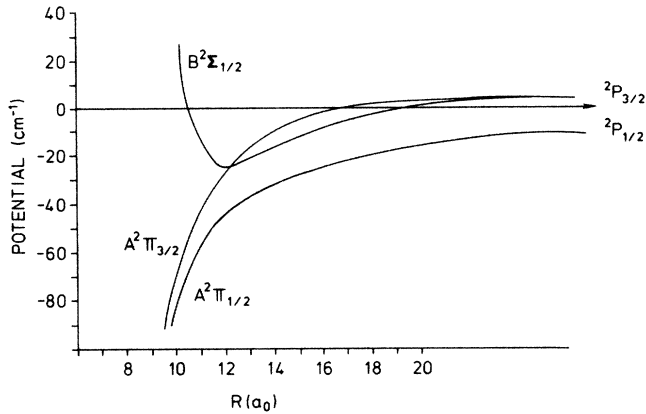


FIG. 2. Na-Ar excited-state potentials obtained by diagonalizing the electronic plus spin-orbit parts of the Hamiltonian ($H^e + H^{so}$) as a function of internuclear separation R .

pure $B\Sigma$ state, while for far-red detunings, the excitation is to a predominately $A\Pi$ state. Under these circumstances, photon absorption is readily understood as $B\Sigma \leftarrow X\Sigma$ or $A\Pi \leftarrow X\Sigma$ molecular transitions.

In case (a), the nonadiabatic dynamics which determine the distribution of final states occur at intermediate internuclear separations where the off-diagonal spin-orbit and rotational terms in the Hamiltonian become comparable to the final-state BO difference potentials. If some representation other than case (a) is used in the R range where absorption occurs, then the photon excitation must be thought of as producing not a single state in this basis, but a coherent mixture of states which are propagated using a strongly nondiagonal Hamiltonian.

B. Distorted-wave analysis

The full radiative, close-coupled scattering calculations, presented in the following section, directly give the desired reduced radiative transition matrix elements S_{fi} . These are all that are required in order to give the full close-coupled results discussed in this paper. However, a distorted-wave analysis of these matrix elements for weak fields is quite helpful in giving some insight into the molecular dynamics between absorption and detection. The desired matrix elements are^{14,21}

$$S_{fi} = -2\pi i (2\pi\hbar\omega\phi/c)^{1/2} \langle \Psi^- | \hat{\mathbf{e}} \cdot \boldsymbol{\mu} | \psi^+ \rangle. \quad (2)$$

$$D(f \leftarrow X^2\Sigma_{1/2}) = [\tilde{N}^-(f, B^2\Sigma_{1/2}) d(B^2\Sigma_{1/2} \leftarrow X^2\Sigma_{1/2}) + \tilde{N}^-(f, A^2\Pi_{1/2}) d(A^2\Pi_{1/2} \leftarrow X^2\Sigma_{1/2}) + \tilde{N}^-(f, A^2\Pi_{3/2}) d(A^2\Pi_{3/2} \leftarrow X^2\Sigma_{1/2})] e^{i\eta_i}. \quad (6)$$

One feature of (6) is that the excitation amplitude $D(f \leftarrow X^2\Sigma_{1/2})$ is made up of a coherent sum of amplitudes from each of the excited electronic states. Of course, choosing the photon frequency allows us to select either predominant Σ or Π excitation. For far-blue-wing detuning, the antistatic $d(\Pi \leftarrow \Sigma)$ excitation amplitude is

Here $|\psi^+\rangle$ is the field-free initial state of given J and parity with incoming boundary conditions and $|\Psi^-\rangle$ is the final state with outgoing boundary conditions. The Hund's case-(e) initial- and final-state indices i and f specify the angular momenta (J_a, l, J) of those states. Quite useful insights on nonadiabatic dynamics may be obtained by examining the structure of the close-coupled wave function. The generalized nonadiabatic Franck-Condon matrix elements in Eq. (2)

$$D_{fi} = \langle \Psi^- | \hat{\mathbf{e}} \cdot \boldsymbol{\mu} | \psi^+ \rangle \quad (3)$$

can be factored into separate parts which exhibit the rate of absorption and the nonadiabatic dynamics. The details of such an analysis are presented elsewhere.¹⁴

As discussed in the previous section, assume that the detuning is in the far wings of the profile so that the point(s) of stationary phase for (3) occur(s) in the case-(a) region. For each initial parity and branch, the transition amplitude matrix \underline{D} above can be approximated by the following factored form:

$$\underline{D} \approx \tilde{N}^- \underline{d} \underline{N}^+. \quad (4)$$

Here, \underline{d} is a matrix of adiabatic Franck-Condon amplitudes with elements

$$d_{fi} = \langle f_f^0 | \mu_{fi} | f_i^0 \rangle, \quad (5)$$

where f^0 represents the ordinary, real, energy-normalized, radial vibrational wave functions for the case-(a) diagonal potentials (that is, the adiabatic, or single-channel, potentials), μ_{fi} represents the molecular transition dipole [here case (a)] and \underline{N}^\pm are, respectively, initial- and final-state dynamical matrices. The d_{fi} terms are adiabatic Franck-Condon amplitudes that carry all the information about the radiative excitation process. The \underline{N}^\pm matrices are independent of the radiation field and contain the information about the field-free molecular dynamics.

For the present problem, \underline{N}^+ is 1×1 , \underline{N}^- is 3×3 , and \underline{d} is 3×1 . There are 18 possible amplitudes D_{fi} for each initial J corresponding to the three possible transition branches for each initial e or f parity. The initial-state matrix \underline{N}^+ is a trivial phase factor $e^{i\eta_i}$, where η_i is the phase shift for elastic scattering on the ground-state potential. The unitary, nondiagonal final-state matrices \underline{N}^- describe the effects of nonadiabatic coupling among the molecular states. The full expression for the transition amplitude is thus

negligible compared to the quasistatic $d(\Sigma \leftarrow \Sigma)$ factor, and vice versa for far-red-wing detuning.

One important feature of our postulated conditions (absorption into a region of uncoupled, or adiabatic, molecular states) is the unitarity of \underline{N}^- .¹⁴ Therefore, the \tilde{N}^- factors in (6) disappear when a summation over final

states is taken:

$$\sum_f |D_{fi}|^2 = \sum_f |d_{fi}|^2. \quad (7)$$

The total absorption coefficient (or equivalently, the total cross section), while is proportional to the sum in (7), is expressed in terms of the adiabatic Franck-Condon matrix elements (5). This presumes, of course, that absorption occurs at stationary-phase points in a region where suitable adiabatic reference potentials can be defined. This condition is normally satisfied in the line wings. Thus, Eq. (7), based on the factorization (4), shows why the simple semiclassical, or quasistatic, wing profiles agree so well with the nonadiabatic quantum close-coupled results; the semiclassical approximation to the adiabatic Franck-Condon factors is quite good for isolated Condon points. This favorable quantum-quasistatic comparison of wing absorption has been demonstrated both for $O(^1S \rightarrow ^1D) + \text{Ar}$ (Ref. 8) and for $\text{Na}(^2P_j \leftarrow ^2S_{1/2}) + \text{Ar}$.¹¹

The introduction of the \underline{N}^- matrix enables us to devise a time-independent "half-collision" quantum-mechanical analog of the time-dependent, semiclassical picture which has been used for "whole-collision" depolarization cross sections.^{26,33} In the present case, the initial-state collision prepares the molecule for absorption. The absorption process is described by the \underline{d} adiabatic Franck-Condon amplitudes, and the nonadiabatic dynamics in the final state is described by \underline{N}^- . The final-state scattering may be viewed as a progression from regions of one Hund's case to another.^{26,33} It is possible to set up time-independent coupled equations for $\underline{N}^-(R)$ which integrate \underline{N}^- from the absorption region, where $\underline{N}^- = \underline{1}^0$, through the regions of nonadiabatic coupling to the asymptotic region where scattering boundary conditions can be applied to extract the desired asymptotic \underline{N}^- matrix.¹⁴ We may thus attempt to obtain either fully quantal solutions, or semiclassical approximations, to the \underline{N}^- matrix. Since our present paper concentrates on our full radiative, scattering, close-coupled results, we defer any detailed analysis of \underline{N}^- to the future. However, there are simple limiting cases for \underline{N}^- which give some insight into the nonadiabatic dynamics.

The simplest approximation to \underline{N}^- is an adiabatic correlation. For example, we could define adiabatic potentials that connect the short-range molecular states to the long-range 2P_j states by diagonalizing the electronic plus spin-orbit Hamiltonian as a function of R . In an adiabatic correlation, \underline{N}^- is diagonal and $B^2\Sigma_{1/2}$, $A^2\Pi_{3/2}$, and $A^2\Pi_{1/2}$ correlate, respectively, with $^2P_{3/2}$, $^2P_{3/2}$, and $^2P_{1/2}$. This leads to branching (as per Sec. III) ratios of 0 for far-blue detuning and 1 for far-red detuning. Such behavior is not observed in our close-coupled calculations, except under special circumstances, so an adiabatic approximation to \underline{N}^- is unsatisfactory for the systems we have examined.

Another simple approximation to \underline{N}^- is to use the recoil limit, which is a "sudden" approximation, applicable at large fragment separation velocity. This limit has been extensively studied recently by Singer *et al.*²⁰ in the context of diatomic photodissociation. There is a close re-

lationship between the theories of laser-assisted collisions and photodissociation.^{14,21} In fact, expression (3) can be used for photodissociation as well, except that the initial-state dynamical matrix \underline{N}^+ is missing and \underline{d} becomes a set of bound-free adiabatic Franck-Condon amplitudes. From the standpoint of final-state dynamics, photodissociation and laser-assisted collisions are treated the same way, and are described by the same \underline{N}^- matrix. In the recoil limit, the atoms are assumed to separate so rapidly that no angular momentum recoupling occurs before the atoms are well separated. The distribution of asymptotic atomic states is thus obtained simply by projecting the molecular state prepared by optical excitation onto the asymptotic channel states. These coefficients are given by a simple unitary transformation, in our case, the (a)→(e) transformation. Singer *et al.*²⁰ were able to show for the special case where one of the product atoms is in an S state that the total fine-structure branching ratios (that is, summed over the $2j+1$ spatial degeneracy of each j state) are statistical. Thus, for our problem, the recoil limit predicts a branching ratio of 0.5, irrespective of whether the detuning is to the red or to the blue, and irrespective of collision partner (He, Ne, or Ar).

Finally, the recoil-limit prediction is not altered by strong nonadiabatic mixing (due to, for example, a curve crossing) occurring at a smaller internuclear separation than the case (a)→(e) transformation region. However, the manner by which the recoil limit is approached (either as a function of scattering energy or detuning) will depend on that mixing.

II. CLOSE-COUPLED EQUATIONS

As the details of the quantum-mechanical close-coupled theory of atomic collisions in a radiation field have been described in several recent papers^{11,30,34,35} we will only present a brief discussion here.

A. Hamiltonian

The Hamiltonian H is given by

$$H = H^{\text{mol}} + H^{\text{rad}} + V^{\text{rad}}, \quad (8)$$

where H^{rad} is the free photon field Hamiltonian and V^{rad} is the dipole interaction operator which couples the molecular and radiative degrees of freedom. The total molecular Hamiltonian, H^{mol} , in barycentric coordinates is given by

$$H^{\text{mol}} = H^e(r, R) + B(R)L_R^2 + H^{\text{so}} + T, \quad (9)$$

where H^e is the electronic Hamiltonian whose eigenvalues are the BO potentials $W_\Lambda(R)$:

$$H^e(r, R)\Psi_e(r, R) = W_\Lambda(R)\Psi_e(r, R). \quad (10)$$

Here r represents the electron coordinates and R is the internuclear separation. T is the kinetic energy operator (relative to the center of mass) and $B(R)L_R^2$ is the rotational operator with $L_R = J - L - S$ and $B(R) = \hbar^2/2\mu R^2$. L and S are the electronic orbital and spin angular momentum operators, while J is the total angular momen-

TABLE I. Elements of the symmetric matrix of the molecular Hamiltonian H^{mol} evaluated in Hund's case (a). The + (−) corresponds to f (e) parity. X' is $J'(J'+1)$ where J' is the final-state angular momentum.

State	Matrix
$X^2\Sigma_{1/2}$	$W_{X\Sigma} + B[X + \frac{1}{4} \mp (X + \frac{1}{4})^{1/2}]$
$B^2\Sigma_{1/2}$	$W_{B\Sigma} + B[X' + \frac{9}{4} \mp (X' + \frac{1}{4})^{1/2}]$
$A^2\Pi_{1/2}$	$(2)^{1/2}B[1 \mp (X' + \frac{1}{4})^{1/2}] + A(2)^{1/2}$
$A^2\Pi_{3/2}$	$-(2)^{1/2}B(X' - \frac{3}{4})^{1/2}$
	$W_{A\Pi} + B(X' + \frac{5}{4}) - A/2$
	$-B(X' - \frac{3}{4})^{1/2}$
	$W_{A\Pi} + B(X' - \frac{3}{4}) + A/2$

tum operator. The phenomenological spin-orbit operator used is

$$H^{\text{so}} = A(R)[L_z S_z + \frac{1}{2}(L_+ S_- + L_- S_+)] \quad (11)$$

and $A(R)$ is the spin-orbit coupling parameter. The dipole operator is given by

$$V^{\text{rad}} = \left[\frac{2\pi\hbar\omega}{c} \phi \right]^{1/2} \hat{\epsilon}_0 \cdot \mathbf{d}, \quad (12)$$

where ϕ is the photon flux and $\hat{\epsilon}_0$ the linear polarization vector of the incident radiation. $\hat{\epsilon}_0$ is taken to be along a space-fixed z axis.

B. Wave functions

We introduce a Hund's case-(a) molecular basis augmented by the radiation field

$$|j\rangle = |JM_p; S\Lambda\Sigma\rangle \otimes |nh\nu, \hat{\epsilon}_0\rangle, \quad (13)$$

where we consider a single-mode radiation field with n photons of frequency ν and a linear polarization vector $\hat{\epsilon}_0$ in the z direction. In this representation, the nonrelativistic electronic Hamiltonian is diagonalized, but both the rotational and spin-orbit Hamiltonians have nonzero off-diagonal terms. The molecular parity is defined with respect to inversion of all particle coordinates so that

$$|JM_p \pm; S\Lambda\Sigma\rangle = (2)^{-1/2} (|JM; S\Lambda\Sigma\rangle \pm |JM; S - \Lambda - \Sigma\rangle) \quad (14)$$

with parity defined by³⁶

$$\begin{aligned} p_- &= (-1)^{J-1/2}, \quad e \text{ parity} \\ p_+ &= (-1)^{J+1/2}, \quad f \text{ parity} \end{aligned} \quad (15)$$

C. Close-coupled equations

For each initial total angular momentum J and parity, we expand the total wave function:⁸

$$\Psi_j(E, R) = |i\rangle F_{ij}(E, R)/R + \sum_f |f\rangle F_{fj}(E, R)/R. \quad (16)$$

Here E is the scattering energy, $|i\rangle$ is the initial state, and the sum over the final states includes all channels that can be reached from the initial state by either radiative or nonradiative transitions. The amplitudes $F_{ii}(R)$ and $F_{ff}(R)$ satisfy coupled radial equations:⁸

$$\begin{aligned} \left(\hbar^2/2\mu \frac{d^2}{dR^2} + E - V_i(R) - nh\nu \right) F_{ii} &= \sum_f V_{if}^{\text{rad}} F_{fi}, \\ \left(\hbar^2/2\mu \frac{d^2}{dR^2} + E - V_f(R) - (n-1)h\nu \right) F_{ff} &= \sum_i V_{fi}^{\text{rad}} F_{if} + \sum_{f' (\neq f)} H_{ff'}^{\text{mol}} F_{f'f}, \end{aligned} \quad (17)$$

where $V_i(R)$ and $V_f(R)$ are the effective Born-Oppenheimer potentials which include centrifugal and diagonal spin-orbit contributions. In evaluating Eq. (17) we use a limited electronic basis set in a case-(a) representation of the initial $X^2\Sigma_{1/2}$ state and final $A^2\Pi_{1/2}$, $A^2\Pi_{3/2}$, and $B^2\Sigma_{1/2}$ states. The matrix elements of H^{mol} for the final-state manifold are presented in Table I. They are diagonal in J , M , and p , and we have assumed, for the purpose of evaluating the matrix elements, that the atomic orbital angular momentum quantum number is a good quantum number.²⁹

The radiative coupling matrix elements V^{rad} couple an initial state (J, p) to final states (J', p') where $pp' = -1$, and $J' = J - 1$ (P branch), $J' = J$ (Q branch), $J' = J + 1$ (R branch). For the space-fixed dipole operator \mathbf{d} , we find

$$\begin{aligned} \langle J'M'p'; S\Lambda'\Sigma' | d_0 | JM_p; S\Lambda\Sigma \rangle \\ = C(J1J'; MOM') \langle J'p'; S\Lambda'\Sigma' | | d | | Jp; S\Lambda\Sigma \rangle, \end{aligned} \quad (18)$$

where the reduced matrix elements are presented in Table II. For sufficiently weak incident laser intensity, the transition amplitudes are linearly dependent on the laser intensity. Thus, the Wigner-Eckart theorem may be used to separate geometric effects into angular momentum algebra and remove the explicit M dependence from the close-coupled equations. The full formalism is discussed in detail by Julienne and Mies²¹ and will not be repeated here.

The coupled equations (17) can be set up and solved using any basis related to the case-(a) basis by an orthogonal transformation. Of course, the asymptotic S matrix must be projected in the asymptotic channel state, or case-(e) basis. Kulander and Rebentrost^{10,11} used the case-(e) basis for setting up their coupled equations. Therefore, our formulation and assumptions are equivalent to theirs, and would lead to the same numerical results, given the same potentials. Our numerical solutions were generated using the same close-coupling scattering code and procedure as that used in Ref. 8. The solution to the unique problems

TABLE II. Reduced e -parity matrix elements of the dipole coupling V^{rad} , evaluated in a Hund's case (a). J is the lower-state angular momentum and the signs in parentheses change the e - to f -parity reduced matrix elements.

Branch	$\langle B^2\Sigma_{1/2} d X^2\Sigma_{1/2} \rangle$	$\langle A^2\Pi_{1/2} d X^2\Sigma_{1/2} \rangle$	$\langle A^2\Pi_{3/2} d X^2\Sigma_{1/2} \rangle$
P	$\left[\frac{2J-1}{4J} \right]^{1/2} \tau_0$	$(-)\left[\frac{2J-1}{8J} \right]^{1/2} \tau_1$	$\left[\frac{(2J-1)(2J-3)}{8J(2J+1)} \right]^{1/2} \tau_1$
Q	0	$(-)\left[\frac{(2J-1)^2}{8J(J+1)} \right]^{1/2} \tau_1$	$\left[\frac{(2J-1)(2J+3)}{8J(J+1)} \right]^{1/2} \tau_1$
R	$-\left[\frac{2J+3}{4(J+1)} \right]^{1/2} \tau_0$	$\left[\frac{(2J+3)}{8(J+1)} \right]^{1/2} \tau_1$	$\left[\frac{(2J+3)(2J+5)}{8(J+1)(2J+1)} \right]^{1/2} \tau_1$

TABLE III. Parameters used in analytical representations of the Na-He, Na-Ne, and Na-Ar (a) $X\Sigma$ and $B\Sigma$ and (b) $A\Pi$ Born-Oppenheimer potentials. (c) contains the Na-Ar CERN parameters. In each case, the internuclear separation R is in atomic units and the potential is in cm^{-1} units. The parameter labels on the right in (b) correspond to Na-Ar only.

	(a)					
	Na-He		Na-Ne		Na-Ar	
	$X\Sigma$	$B\Sigma$	$X\Sigma$	$B\Sigma$	$X\Sigma$	$B\Sigma$
a_1	0.492	0.338	0.492	0.273	0.472	0.313
a_2	0.477	0	-0.024	0	0.137	-0.595
a_3	4.419		5.233		5.444	7.594
a_4	2.999	0.0292	0.483	0.292	0.882	1.516
D_e	2.38	0.51	9.37	4.408	41.00	32.00
R_e	12.00	19.00	10.00	14.50	9.437	12.86
	(b)					
	Na-He	Na-Ne	Na-Ar			
	$A\Pi$	$A\Pi$	$A\Pi$			
C_0	4.03	4.04	4.841	p		
C_6	16.55	13.64	5.75	R_e		
C_8	-3.11	-3.25	510.481	D_0		
C_{10}	0.12	0.09	-0.454	b_2		
D_0	4.04×10^7	4.04×10^7	0.301	b_3		
			0.297	b_4		
			-0.235	b_5		
			0.059	b_6		
	(c)					
	Na-He	Na-Ne	Na-Ar			
	$X\Sigma$	$B\Sigma$	$A\Pi$			
X_1 (10^6)	0.2921	2.876	1.1430			
X_2	0.7458	0.8155	0.9867			
X_3 (10^8)	0.4035	1.2720	0.7061			
X_4 (10^{11})	0.2139	0.6326	0.0692			
X_5 (10^{11})	-0.1202	-0.4263	-0.1501			
X_6	1.1560	2.1720	1.4610			
X_7	5.9920	4.6700	4.9640			
X_8	0.6768	0.8435	0.7856			
X_9	8.0710	6.1440	5.3770			

associated with the presence of nonvanishing asymptotic radiative couplings in optical collisions are described in the Appendix of Ref. 21.

D. Potentials and transition moments

To proceed with the determination of the cross sections, we specify the particular BO potentials and dipole transition moments used in our numerical codes. We use two different fits to the Na-Ar (Ref. 37) numerical potentials, and one for Na-He (Ref. 38) and Na-Ne.³⁹

One particular set of potentials for Na-Ar is obtained by using a European Organization for Nuclear Research (CERN) parameter-fitting routine, MINUET. We specify the generic form

$$V(R) = X_1 e^{-X_2 R} - \frac{\alpha X_3}{R^6} - \beta \frac{X_4}{R^8} - \frac{X_5}{R^{10}}, \quad (19)$$

where

$$\alpha = \frac{1}{1 + \exp[-X_6(R - X_7)]},$$

$$\beta = \frac{1}{1 + \exp[-X_8(R - X_9)]},$$

and fix the R^{-6} coefficient to give the correct asymptotic representation as $R \rightarrow \infty$. The particular parameter values so determined are listed in Table III.

An alternate representation of the ground and excited Σ potentials also used had the form

$$V_{\Sigma}(R) = D_e \{1 - \exp[-a_1(R - R_e)]\}^2 \times \{1 - a_2 \exp[-(R - a_3)^2/a_4^2]\} - D_e \quad (20)$$

with coefficients a_1 , a_2 , a_3 , and a_4 determined by a standard least-squares fit. D_e is the dissociation energy and R_e is the equilibrium position. For Na-Ar, we use the numerical potentials of Saxon *et al.*,³⁷ while for Na-He, we use the theoretical potentials of Pascale,³⁸ and for Na-Ne, the potentials of Peach.³⁹ For Na-Ar, the $A\Pi$ BO potential is fitted to a Thakkar potential⁴⁰

$$V_{\Pi}(R) = D_0 [1 - (R_e/R)^p] \times \left[1 + \sum_{i=2}^6 b_i (1 - R_e/R)^i \right] - D_e \quad (21)$$

with the dissociation energy

$$D_e = D_0 \left[1 + \sum_{i=2}^6 b_i \right]. \quad (22)$$

The coefficients b_i and the parameters D_0 , D_e , and p are obtained by a least-squares fit.

For Na-He and Na-Ne, we use

$$V_{\Pi}(R) = D_0 \exp(-C_0 R) - C_6/(10R)^6 - C_8/(10R)^8 - C_{10}/(10R)^{10}. \quad (23)$$

The transition dipole moments τ_0 and τ_1 are taken from the Na-Ar calculations of Laskowski *et al.*⁴¹ The dipole moments are nearly equal and have an approximately constant value of 2.6 a.u. over the range of internuclear separations of interest; they are nearly equal to that of the

atomic Na $3s$ - $3p$ transition (2.52 a.u.). The fine-structure coupling coefficient $A(R)$ is treated as constant and equal to its atomic Na value of 11.46 cm^{-1} . On the basis of spectroscopic studies, this is an excellent approximation for Na-Ne,⁴² and we have applied it also to the electronically similar Na-Ar and Na-He molecules. The *ab initio* calculation of Cooper⁴³ of $A(R)$ for Na-Ar also supports this approximation at distances $R > 9a_0$, the range of internuclear separations of interest to us. Spectroscopic results^{44,45} indicate that $A(R)$ is not constant ($\sim 10\%$) for smaller internuclear separations than those important for the fine-structure transition process of interest here. Numerical values of the parameters used in $V_{\Sigma}(R)$ and $V_{\Pi}(R)$ are summarized in Table III. The BO potentials used are illustrated in Fig. 1.

III. RESULTS AND DISCUSSION

In the numerical computation of the cross sections $\sigma(j)$, it is convenient to calculate the P -, Q -, and R -branch partial cross sections for each contributing lower-state angular momentum J and parity p . Most of the computations were done at a single scattering energy of 200 cm^{-1} and for a detuning range extending from 500 cm^{-1} blue to 150 cm^{-1} red of the center of gravity of the Na $3p$ multiplet. The scattering energy of 200 cm^{-1} corresponds closely to kT , with T the temperature in recent measurements^{6,46} of fine-structure branching ratios on the systems considered here. The intensity of the incident radiation field was taken to be 1 kW/cm^2 . This is a weak field for far-wing excitation and numerically we found that the cross section depended linearly on the incident laser intensity. In all runs, convergence in J was easily achieved, allowing truncation of the infinite J series occurring in $\sigma(j)$.

Our most extensive results are for Na-Ar, and we present those first. In particular, we have also calculated the energy dependence of $\sigma(j)$ for a blue detuning of 100 cm^{-1} with energy E ranging from threshold to 2000 cm^{-1} , allowing us to study the energy-dependent approach to the recoil limit²⁰ discussed in Sec. I B. We then present our results for Na-Ne and Na-He and compare them to those of Na-Ar. In order to facilitate comparisons with experimental data, it will be convenient to present our results as a normalized absorption coefficient⁸ $K(j) = \sigma(j)v/\phi$ or as a branching ratio $B(\Delta) = K(j=1/2)/K(j=3/2)$. Here v is the initial relative scattering velocity and ϕ is the photon flux. Note that if α denotes the Beer's law absorption coefficient then K is simply the normalized absorption coefficient $\alpha/[\text{Na}][\text{RG}]$; $[X]$ represents the density of species X . Note also that in this report detunings Δ are measured relative to the center of gravity of the Na $3p$ multiplet.

A. Na-Ar results

1. J dependence

Typically, the partial cross sections $\sigma_J(j)$ display an oscillatory dependence on J , as shown in Fig. 3. These oscillations, which arise through the J dependence of the excitation amplitudes, depend on detuning and collision en-

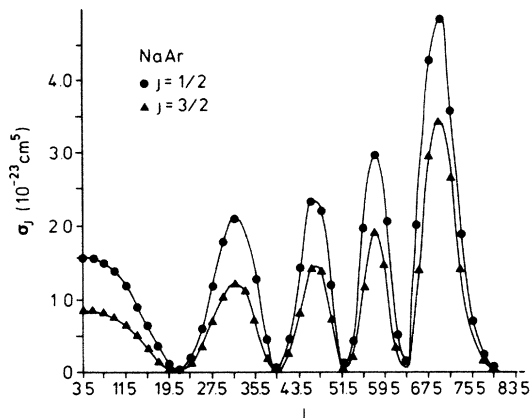


FIG. 3. Na-Ar partial cross section $\sigma_j(j)$ for the P branch and f parity. $E = 200 \text{ cm}^{-1}$ and $\Delta = 100 \text{ cm}^{-1}$.

ergy. It should be noted that a shape or Feshbach-type resonance⁴⁷ in $\sigma_j(j)$ can occur at certain collision energies. At these resonances, the entire cross section can be dominated by the contribution from a single J . We discuss resonances in a later section.

The cutoff in σ_j around $J_m = 79.5\hbar$ has an elementary semiclassical explanation. Indeed, for a particular detuning, there is typically a narrow range of internuclear separations, centered at R^* , over which optical transitions take place. For collision energy E , velocity v , and reduced mass μ , this limits the maximum impact parameter such that $J_m = \mu v R^* / \hbar$. This estimate of J_m quite accurately predicts the numerically determined cutoff J_m in the cross sections for all three Na-RG systems considered here.

2. Parity dependence

The total cross section $\sigma(j)$ can be calculated from the sum of partial cross sections for each branch and initial parity. We find that for each branch (P, Q, R) the partial cross section depends strongly on parity, Fig. 4. The

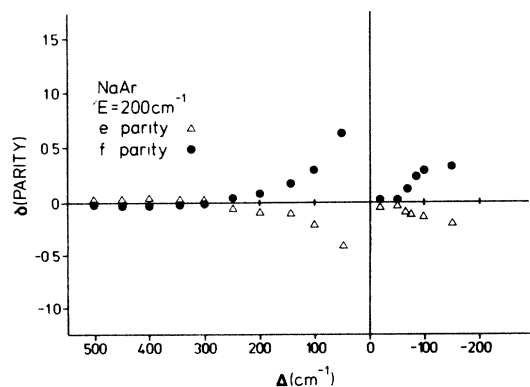


FIG. 4. Differential contributions to Na-Ar $K(j=1/2)$ from states of e and f parity as a function of detuning Δ . $E = 200 \text{ cm}^{-1}$.

quantity δ (parity) is defined as the difference divided by the sum. The origin of this parity dependence can be seen from Tables I and II which exhibit large parity-dependent diagonal and off-diagonal terms in the case-(a) Hamiltonian. Thus, both excitation (V^{rad}) and propagation (H^{mol}) contribute to the parity dependence of $\sigma(j)$. An examination of the table reveals that the ${}^2\Pi_{1/2}-{}^2\Sigma_{1/2}$ coupling matrix element at the curve crossing is different for each parity:

$$(2)^{1/2}B\{1 \mp [J(J+1) + \frac{1}{4}]^{1/2}\} + (2)^{-1/2}A, \quad (24)$$

with upper (lower) sign for the e (f) parity. A is the spin-orbit coupling parameter. If these matrix elements are used in a Landau-Zener⁴⁸ model for the curve crossing near $12.2a_0$ in the BO potentials for Na-Ar (Fig. 1), we see that the diabatic transition probability increases with J for f parity, but decreases for e parity. The J dependence of the e - f parity differences in $\sigma(j)$ obtained from this model is in general qualitative agreement with the numerical close-coupling calculations. The A ${}^2\Pi_{3/2}-A$ ${}^2\Pi_{1/2}$ rotational coupling is not parity dependent.

3. Energy dependence E and the recoil limit

The energy dependence of $K(j)$ is presented in Fig. 5 for a blue detuning of 100 cm^{-1} . The total $K(1/2) + K(3/2)$ is constant at high E in accordance with the predictions of the quasistatic theory.^{11,27} The cross section itself decreases with increasing E since it is proportional to $1/v$.¹¹ Physically, this decrease can be considered to be due to a decrease in the average collision time, with a corresponding decrease in the probability of photon absorption during the collision.

The $K(j)$ for blue detuning vary smoothly with E . There is some resonance structure (not shown) at very small E associated with resonances (quasibound levels) in the shallow $X\Sigma$ and $B\Sigma$ potentials. However, $K(j)$ for red detuning (not shown) exhibits a considerable amount of complex structure at low E due to the increased importance of quasibound levels for the deeper $A\Pi$ potentials. Figure 6 illustrates how a single resonance for $J=49.5\hbar$ is principally responsible for a strong narrow resonance feature near $E=71.975 \text{ cm}^{-1}$ for a red detuning of 50

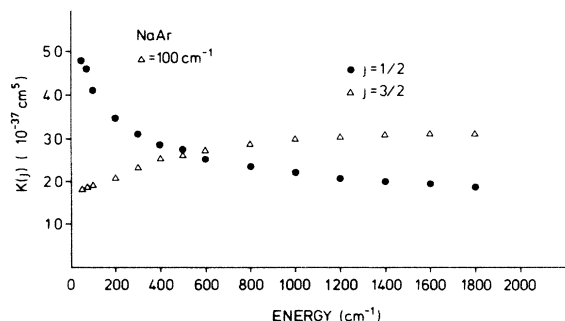


FIG. 5. Energy dependence of Na-Ar absorption coefficient $K(j)$ for detuning $\Delta = 100 \text{ cm}^{-1}$.

cm^{-1} . The presence of other (relatively weaker) resonance contributions to the sum is also evident in Fig. 6. In general, the resonance structure is very complex and our computations are on too coarse a grid to map these features accurately. Some resonances are several cm^{-1} in width while others are very narrow ($<0.01 \text{ cm}^{-1}$). The total cross sections can vary by orders of magnitude, making a detailed survey extremely difficult. An estimate of the contribution of quasibound resonances to the thermally averaged spectrum shows that their overall influence is relatively minor in the present case due to the limited phase space available to the resonances.⁴⁹

The resonances are in some instances $A^2\Pi_{1/2}$ shape resonances, while in others they are $A^2\Pi_{3/2}$ resonances predissociating to the $A^2\Pi_{1/2}$ state. An interesting feature of the resonances is their propensity to decay almost entirely to the asymptotic $^2P_{1/2}$ state even when the total energy is above the $^2P_{3/2}$ asymptote. As the near-threshold excess energy is virtually all potential (rotational), resulting in slow radial dissociation, this behavior is likely due to adiabatic adjustment of the motion to the $A^2\Pi_{1/2}$ state, with a corresponding adiabatic correlation to the $^2P_{1/2}$ state.

At sufficiently high separation velocities, the recoil limit²⁰ should predict the fine-structure branching ratio. In this limit, the branching ratio, $K(1/2)/K(3/2)$, for our case will be 0.5, irrespective of collision partner. We expect this to occur when the separation time $\Delta R_s/v$ is much shorter than a characteristic time of spin-orbit coupling, say $\hbar/\Delta E$. Here ΔR_s is some characteristic separation distance from the case-(a) absorption region to the separated atoms and we take ΔE to be the asymptotic atomic Na $^2P_{3/2}$ - $^2P_{1/2}$ energy difference. If we apply the criterion $v \gg \Delta E \Delta R_s / \hbar$ and use $\Delta R_s = 7a_0$ we require the relative separation velocity $v \gg 1.2 \times 10^5 \text{ cm s}^{-1}$. Thus the final-state collision kinetic energy must be much greater than 800 cm^{-1} for Na-Ar and much greater than 200 cm^{-1} for Na-He. Since the final-state total energy

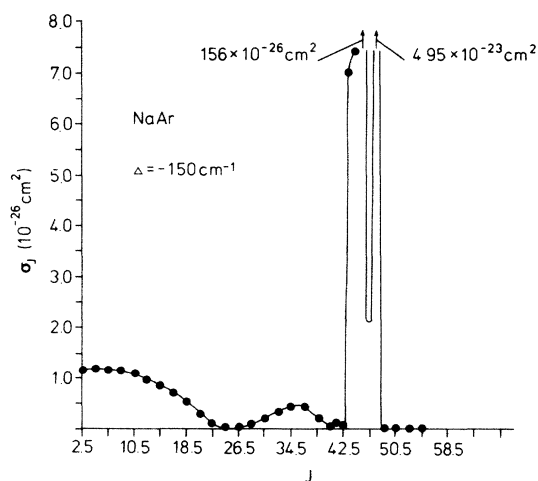


FIG. 6. Na-Ar partial cross section $\sigma_j(j=1/2)$ for the $E=71.975 \text{ cm}^{-1}$ resonance at $\Delta=-50 \text{ cm}^{-1}$. Note that the resonance at $J=49.5\hbar$ is one unit of J wide and about 10^3 stronger than the resonance at $J=45.5\hbar$.

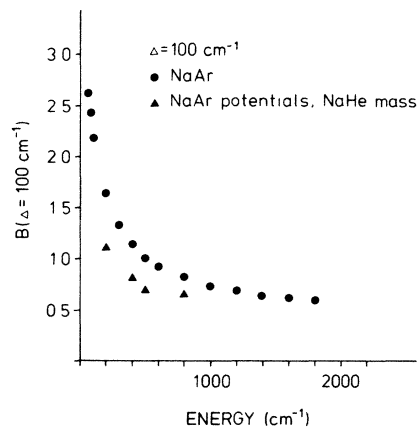


FIG. 7. Approach of branching ratio $B(\Delta)$ to the recoil limit for $\Delta=+100 \text{ cm}^{-1}$. Na-Ar and Na-Ar with Na-He reduced mass.

$E'=E+\Delta$, the recoil limit may be approached for red- or blue-wing detunings by increasing the initial-state scattering energy E . In Fig. 7 we show the energy dependence of the Na-Ar branching ratio $B(\Delta)$ for a blue detuning of $\Delta=100 \text{ cm}^{-1}$. As discussed in previous paragraphs, while there is considerable low-energy variation in $B(\Delta)$, the branching ratio indeed approaches the recoil limit of 0.5 for large E . A similar approach to the recoil limit, with increasing energy E' , is found for far-red-wing detuning. In this case the ratio B is less than 0.5 for low E' and increases to 0.5 as E' increases.

An informative test of the effects of the mass of the collision partners is to calculate the energy dependence of $B(\Delta)$ for $\Delta=100 \text{ cm}^{-1}$ using the potentials for Na-Ar, but the reduced mass of Na-He. These results are also shown in Fig. 7 where we see that in fact the recoil limit is approached for much lower velocity and the departures from the recoil limit are smaller than for the normal calculation with the Na-Ar reduced mass. The same effect is found for red detuning. Note that this result is consistent with the photodissociation calculation of Singer *et al.*¹⁸ for Na-H. Although the Na-H potentials are much different than those for the Na-RG molecules, they found that the recoil limit for the Na 2P branching ratio was reached for about 200 cm^{-1} of separation kinetic energy.

The model calculations with Na-Ar potentials and Na-He mass do, for $\Delta=100 \text{ cm}^{-1}$, show small departures from the recoil limit at high velocity. It is apparent from examining the transition amplitudes [see Eq. (6)] that significant Σ - Π interference is occurring at $\Delta=100 \text{ cm}^{-1}$ between the quasistatic Σ -wing and the antistatic Π -wing excitation amplitudes. In fact, for this detuning and for 2000 cm^{-1} of recoil kinetic energy, there is only about a factor of 5 difference between the Σ and Π excitation amplitudes (a factor of 25 in Σ - Π absorption coefficients). For a larger detuning of $\Delta=300 \text{ cm}^{-1}$ the interference was greatly decreased and the recoil limit approached more closely.

4. Branching ratios and total cross sections

The normalized absorption coefficient⁸ $K(j)$ for Na-Ar as a function of detuning (at energy $E=200\text{ cm}^{-1}$) is shown in Fig. 8. The substantial difference between $K(1/2)$ and $K(3/2)$ as a function of Δ and the strong red-blue asymmetry in these differences are indicative of the nonadiabatic mixing in the excited states. The asymmetry may be brought out more clearly, and more readily compared to experiment, by calculating a branching ratio $B(\Delta)=K(1/2)/K(3/2)$. This is shown in Fig. 9 for $E=200\text{ cm}^{-1}$. The ratio is a direct measure of the relative population produced in the Na $^2P_{1/2}$ and $^2P_{3/2}$ states. For now we note that in an adiabatic limit $B(\Delta)=0$ for far-blue detuning ($\Delta \gg 0$), when excitation is to the $B^2\Sigma$ state, while $B(\Delta)\simeq 1$ for red detuning ($\Delta \ll 0$). In the recoil limit $B(\Delta)=0.5$ for either detuning. In Sec. III C we discuss, through comparisons of our results for Na-Ar, Na-Ne, and Na-He optical collisions, the sensitive dependence of the branching ratios on the interatomic potentials.

In Fig. 9, we compare the branching ratio $B(\Delta)$, at $E=200\text{ cm}^{-1}$, with recent experimental data.^{15,46} The overall agreement is quite good, particularly considering the energy dependence of $\sigma(1/2)$ and $\sigma(3/2)$. We also present in Fig. 9 for $\Delta=100\text{ cm}^{-1}$ a thermally averaged branching ratio which is in good agreement with the experiment. The recent Na-Ar theoretical calculations of Kulander *et al.*,¹¹ done at a scattering energy $E=219.47\text{ cm}^{-1}$, are also presented in the figure. These authors also used a fully quantum-mechanical approach, but numerically solved the full 10×10 set of differential equations. They used the Na-Ar potentials of Duren *et al.*,⁵⁰ which are similar, in the asymptotic region, to those used in our calculations. The good correspondence between their calculations of $B(\Delta)$ and ours is evident from the figure. The difference may be attributed to the strong energy dependence of $B(\Delta)$ (see Fig. 7) and to the different

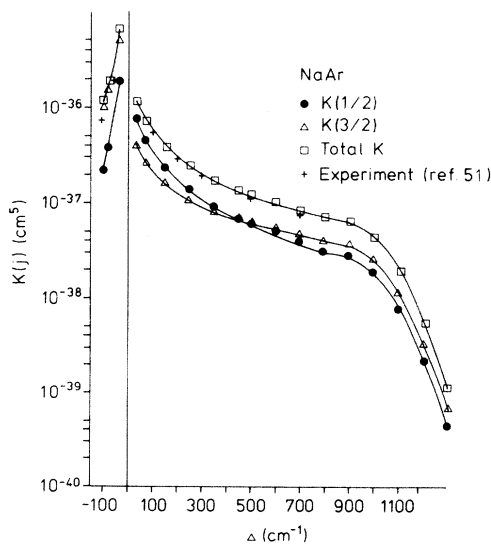


FIG. 8. Na-Ar normalized absorption coefficients for production of Na($3p$) atoms vs detuning: $K(1/2)$ and $K(3/2)$, $K(1/2)+K(3/2)$. $E=200\text{ cm}^{-1}$.

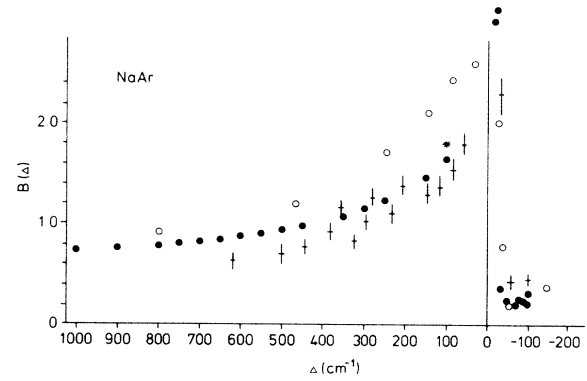


FIG. 9. Detuning dependence of the branching ratio $B(\Delta)$ for Na-Ar. $E=200\text{ cm}^{-1}$. Our calculations (\bullet); calculations of Ref. 11 (\circ); experimental data of Refs. 15 and 46 ($+$). Thermal average of our calculations for $\Delta=100\text{ cm}^{-1}$ ($*$).

potentials used in the two calculations.

While the size of the branching ratio $B(\Delta)$ is principally sensitive to the shape of the BO $A\Pi-B\Sigma$ difference potentials, the total normalized absorption $K(1/2)+K(3/2)$ is sensitive to $X\Sigma-A\Pi$ and $X\Sigma-B\Sigma$ difference potentials. In Fig. 8, we also compare the total (quantum-mechanical) calculated normalized absorption profile to the experimental one of Jongorius,⁵¹ which is consistent with other experimental determinations.^{52,53} The good agreement with our results is evident, and attests to the quality of the potentials used in our calculations.

B. Na-He and Na-Ne results

1. J dependence

The partial cross sections for Na-He and Na-Ne also exhibit oscillatory dependence on J , but due to the reduced-mass dependence of J_m , we find

$$J_m(\text{Na-He}) < J_m(\text{Na-Ne}) < J_m(\text{Na-Ar}).$$

2. Parity dependence

The parity dependence of the partial cross sections for Na-He and Na-Ne is similar to that for Na-Ar, as shown in Fig. 10.

3. Cross sections and branching ratios

Here we see a strong red-blue asymmetry, but in a sense opposite to that for Na-Ar. Here for the blue wing $K(3/2) > K(1/2)$ while generally $K(1/2) \sim K(3/2)$ on the red wing. Those differences are clearly brought out in the branching ratios $B(\Delta)$ for Na-He and Na-Ne optical collisions; these are presented in Fig. 11 for a single scattering energy $E=200\text{ cm}^{-1}$ and compared to recent experimental data.⁴⁶ As discussed in the following section the difference between the Na-Ar case and that of Na-He and Na-Ne is likely due to the considerably greater attraction of the Na-Ar $B\Sigma$ potential.

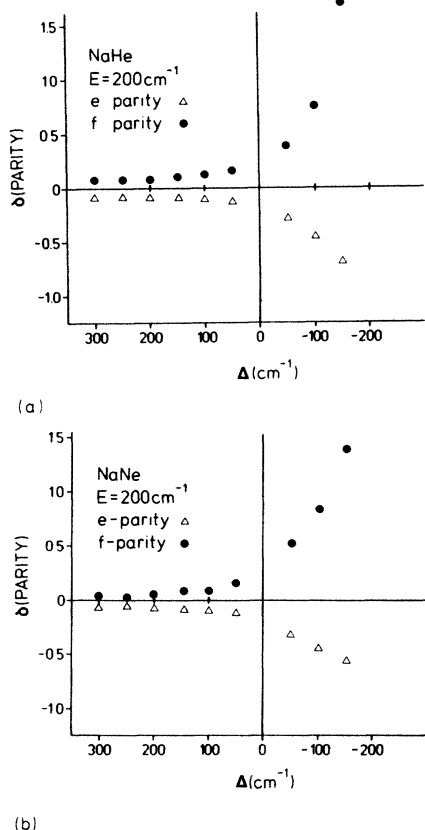


FIG. 10. Contributions to Na-He and Na-Ne $K(j=1/2)$ from states of e and f parity as a function of detuning Δ . $E=200\text{ cm}^{-1}$.

C. Discussion

In this section we discuss the general detuning dependence of the branching ratio $B(\Delta)$ and contrast its behavior for the Na-He, Na-Ne, and Na-Ar molecules. The qualitative features of $B(\Delta)$ may be understood as follows. For detunings far into the blue wing final-state scattering energy is increasing with Δ . Excitation is to a

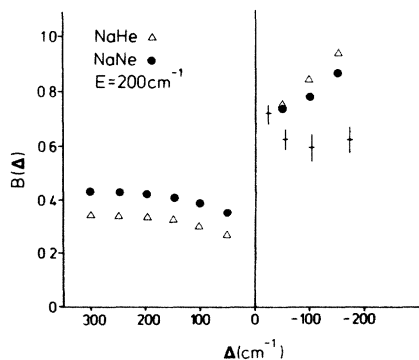


FIG. 11. Branching ratio $B(\Delta)$ vs Δ for Na-He and Na-Ne at $E=200\text{ cm}^{-1}$. Our calculations (●); Na-He experimental data of Ref. 46 (†).

predominately $B\Sigma$ state with the contribution from the antistatic $A\Pi$ state wing decreasing rapidly with Δ . The situation approximates the recoil limit discussed previously, and we expect $B(\Delta)$ to approach 0.5 in the far blue wing, irrespective of collision partner. In the near blue wings the Σ - Π spin-orbit coupling becomes important, as do the detailed shapes of the $A\Pi$ and $B\Sigma$ potentials (Fig. 1). For Na-Ar, the relatively strong attraction in the $B\Sigma$ state ($\gg A$) produces a reversal of $B(\Delta)$ from expectations based on adiabatic correlation to the atomic Na $3p$ states (Fig. 2). The projection of the Na-Ar roots of the diagonalized electronic-rotational Hamiltonian (Fig. 12) onto the case-(a) basis in the vicinity of the curve crossing clearly displays the strong $B^2\Sigma_{1/2}-A^2\Pi_{1/2}$ diabatic transition that produces the reversal. $B(\Delta)$ thus approaches the recoil limit, with increasing Δ , from above 0.5. For Na-He and Na-Ne, on the other hand, the $B\Sigma$ state attraction is weak ($\ll A$), resulting in considerably less likelihood of a diabatic $B^2\Sigma_{1/2}-A^2\Pi_{1/2}$ transition compared to the Na-Ar case. The smaller diabatic transition probability is reflected in the approach (with increasing Δ) of $B(\Delta)$ to the recoil limit from below 0.5 for Na-He and Na-Ne.

In the vicinity of the impact region (within a few cm^{-1}) of the atomic Na $^2S_{1/2}-^2P_{3/2}$ state, resonant excitation dominates wing excitation of the $^2P_{1/2}$ state, and $B(\Delta)$ becomes small for each Na-RG case. In contrast, within the impact region of the Na $^2S_{1/2}-^2P_{1/2}$ transitions $B(\Delta)$ becomes large, due to direct excitation of the $^2P_{1/2}$ state. However, the effect of inelastic collisions is not negligible even in the impact region and they produce finite $B(\Delta)$ even for resonant excitation. The details of our studies of

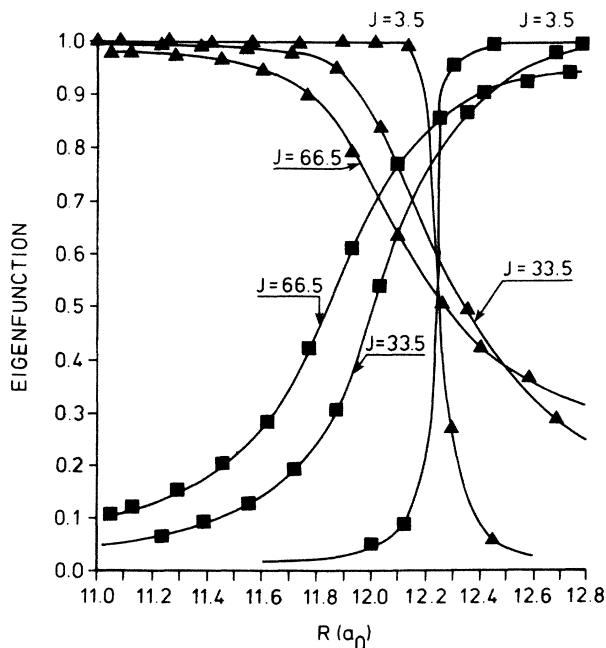


FIG. 12. Projection of the Na-Ar roots of the diagonalized electronic-rotational matrix onto a Hund's case-(a) basis as a function of internuclear separation. The detuning is 100 cm^{-1} , $E=200\text{ cm}^{-1}$, and the data are for the P branch. $B^2\Sigma_{1/2}$ (▲); $A^2\Pi_{1/2}$ (■). The curves through the data are to guide the eye.

the region between the D lines and in the line cores will be presented in a future report.

In the red wings excitation is principally to the $A\Pi$ state. The $A^2\Pi_{3/2}$ component of this state correlates adiabatically to the $^2P_{3/2}$ state, while the $A^2\Pi_{1/2}$ component correlates to the $^2P_{1/2}$ state. The $A^2\Pi_{3/2}$ state is coupled only weakly by rotation to the $A^2\Pi_{1/2}$ state. In contrast to the blue-wing results we then have small branching ratios where the $A^2\Pi_{1/2}-B^2\Sigma_{1/2}$ coupling is strong (as in Na-Ar) and larger branching ratios where it is weak (as in Na-He and Na-Ne). Further into the red wings $B(\Delta)$ varies rapidly as a result of scattering resonances in the $A\Pi$ state. Near threshold the Na $^2P_{3/2}$ channel closes for a scattering energy 17.196 cm^{-1} higher than for the Na $^2P_{1/2}$ channel; this results in a rapid increase in $B(\Delta)$ in this region.

IV. CONCLUSIONS

In conclusion, we have carried out fully quantum-mechanical calculations of fine-structure branching cross

sections for Na-He, Na-Ne, and Na-Ar optical collisions. We obtain good agreement with available experimental data^{15,46} and with previous Na-Ar calculations by Kullander *et al.*^{10,11} The calculations indicate that the recoil limit²⁰ gives correct branching ratios for sufficiently high separation velocity and that, even for molecules with identical BO potentials, the approach to the recoil limit is mass dependent. Low-velocity collisions show large departures from the simple recoil limit and from an adiabatic limit. These are a consequence of the detailed non-adiabatic dynamics and are a measure of the influence of the interatomic potentials and nonadiabatic couplings.

ACKNOWLEDGMENTS

We acknowledge the assistance of F. T. Delahanty in acquiring some of the experimental data presented in this paper. This work was supported by the National Science Foundation (Grant No. PHY-8305752) and the Air Force Office of Scientific Research (Grant No. AFOSR-ISSA-85-0045).

*Current address: Old Dominion University, Department of Electrical Engineering, Norfolk, VA 23508.

¹P. Thomann, K. Burnett, and J. Cooper, *Phys. Rev. Lett.* **45**, 1325 (1980).

²K. Burnett, J. Cooper, R. J. Ballagh, and E. W. Smith, *Phys. Rev. A* **22**, 2005 (1980).

³K. Burnett and J. Cooper, *Phys. Rev. A* **22**, 2027 (1980); **22**, 2044 (1980).

⁴V. Kroop and W. Behmenberg, *Z. Phys. A* **294**, 299 (1980).

⁵W. J. Alford, K. Burnett, and J. Cooper, *Phys. Rev. A* **27**, 1310 (1983).

⁶M. D. Havey, G. E. Copeland, and W. J. Wang, *Phys. Rev. Lett.* **50**, 1767 (1983).

⁷N. Böwering, T. D. Raymond, and J. W. Keto, *Phys. Rev. Lett.* **52**, 1880 (1984).

⁸P. S. Julienne, *Phys. Rev. A* **26**, 3299 (1982).

⁹P. S. Julienne, in *Proceedings of the Sixth International Conference on Spectral Line Shapes, Boulder, Colorado, 1982*, edited by K. Burnett (de Gruyter, Berlin, 1982), Vol. II.

¹⁰K. C. Kulander and F. Reberstrost, *Phys. Rev. Lett.* **51**, 1262 (1983).

¹¹K. C. Kulander and F. Reberstrost, *J. Chem. Phys.* **80**, 5623 (1984).

¹²K. Burnett, *Comments At. Mol. Phys.* **13**, 179 (1983).

¹³K. Burnett, in *Proceedings of the Seventh International Conference on Spectral Line Shapes, Aussois, France, 1984*, edited by F. Rostas (de Gruyter, Berlin, 1984), Vol. III.

¹⁴F. H. Mies and P. S. Julienne, in Ref. 13; Paul S. Julienne and Frederick H. Mies, in *Electronic and Atomic Collisions*, edited by D. C. Lorentz, W. E. Meyerhof, and J. R. Petersen (North-Holland, Amsterdam, 1986).

¹⁵M. D. Havey and L. L. Vahala, in Ref. 13.

¹⁶L. Klein, B. Talin, V. Kaftandjian, and R. Stamm, in Ref. 13.

¹⁷E. W. Rothe, U. Krause, and R. Duren, *Chem. Phys. Lett.* **72**, 100 (1980).

¹⁸S. J. Singer, K. F. Freed, and Y. B. Band, *Chem. Phys. Lett.* **91**, 12 (1982).

¹⁹W. S. Struve, S. J. Singer, and K. F. Freed, *Chem. Phys. Lett.* **110**, 588 (1984).

²⁰S. J. Singer, K. F. Freed, and Y. B. Band, *J. Chem. Phys.* **81**, 3064 (1984).

²¹P. S. Julienne and F. H. Mies, *Phys. Rev. A* **30**, 831 (1984).

²²H. Kato and K. Onomichi, *J. Chem. Phys.* **82**, 1642 (1985).

²³G. Nienhuis, *J. Phys. B* **16**, 1 (1983).

²⁴K. Burnett, *Phys. Rep.* **118**, 1 (1985).

²⁵Alain Omont, in *Progress in Quantum Electronics 5* (Pergamon, New York, 1977).

²⁶F. Masnou-Seeuws and R. McCarroll, *J. Phys. B* **7**, 2230 (1974).

²⁷R. E. Hedges, D. Drummond, and A. Gallagher, *Phys. Rev. A* **6**, 1519 (1972).

²⁸G. Herzberg, *Spectra of Diatomic Molecules*, 2nd ed. (Van Nostrand, Princeton, 1950).

²⁹J. T. Hougen, *Natl. Bur. Stand. (U.S.) Monograph No. 115* (U.S. GPO, Washington, D.C., 1970).

³⁰F. H. Mies, in *Theoretical Chemistry: Advances and Perspectives*, edited by Douglas Henderson and Henry Eyring (Academic, New York, 1981), Vol. 6B.

³¹F. H. Mies, *Phys. Rev. A* **7**, 942 (1973).

³²F. H. Mies, *Mol. Phys.* **41**, 973 (1980).

³³E. E. Nikitin, in *The Excited State in Chemical Physics* (Wiley, New York, 1975).

³⁴P. L. DeVries and T. F. George, *Mol. Phys.* **36**, 151 (1978).

³⁵P. L. DeVries and T. F. George, *Mol. Phys.* **38**, 56 (1979).

³⁶J. M. Brown, J. T. Hougen, K. P. Huber, J. W. C. Johns, I. Kopp, H. Lefebvre-Brion, H. J. Merer, D. A. Ramsay, J. Rostas, and R. N. Zare, *J. Mol. Spectrosc.* **55**, 500 (1975).

³⁷R. P. Saxon, R. E. Olson, and B. Liu, *J. Chem. Phys.* **67**, 2692 (1977).

³⁸J. Pascale, *Phys. Rev. A* **28**, 632 (1983).

³⁹G. Peach, *Comments At. Mol. Phys.* **11**, 101 (1982).

⁴⁰A. J. Thakkar, *J. Chem. Phys.* **62**, 1693 (1975).

⁴¹B. C. Laskowski, S. R. Langhoff, and J. R. Stallcop, *J. Chem. Phys.* **75**, 815 (1981).

⁴²R. A. Gottscho, R. Ahmad-Bitar, W. P. Lapatovich, I. Renhorn, and D. E. Pritchard, *J. Chem. Phys.* **75**, 2546 (1981).

⁴³D. L. Cooper, *J. Chem. Phys.* **75**, 4157 (1981).

- ⁴⁴R. E. Smalley, D. A. Auerbach, P. S. H. Fitch, D. H. Levy, and L. Wharton, *J. Chem. Phys.* **66**, 3778 (1977).
- ⁴⁵A. Marjatta Lyyra, W. P. Lapatovich, P. E. Moskowitz, M. D. Havey, R. Ahmad-Bitar, R. A. Gottscho, and D. E. Pritchard (unpublished).
- ⁴⁶M. D. Havey, F. T. Delahanty, L. L. Vahala, and G. E. Copeland, *Phys. Rev. A* (to be published).
- ⁴⁷H. Feshbach, *Ann. Phys. (N.Y.)* **5**, 357 (1958).
- ⁴⁸C. Zener, *Proc. R. Soc. London, Ser. A* **137**, 696 (1932).
- ⁴⁹G. York, R. Scheeps, and A. Gallagher, *J. Chem. Phys.* **63**, 1052 (1975).
- ⁵⁰R. Duren, E. Hasselbrink, and G. Moritz, *Z. Phys. A* **307**, 1 (1982).
- ⁵¹M. J. Jongerius, Tj. Hollander, and C. Th. Alkemade, *J. Quant. Spectrosc. Radiat. Transfer* **26**, 285 (1981).
- ⁵²D. G. McCartan and J. M. Farr, *J. Phys. B* **9**, 985 (1976).
- ⁵³W. P. West and Alan Gallagher, *Phys. Rev. A* **17**, 1431 (1978).